Galaxy evolution with J-PAS

Bonoli, S.[1,2], **Acharya, N.**[1], **Cortesi, A.** [3] **Díaz-García, L. A.**[4], **González Delgado, R. M.**[4], **Iglesias-Páramo, J.**[4], **López, I. E.** [5] **Rahna, P. T.** [6] **Rodríguez-Martín, J. E.,** [4] **Torralba, A.**[7,8], **Abramo, R.**[9], **Alcaniz, J.**[10], **Benitez, N., Carneiro, S.**[11], **Cenarro, J.**[6], **Cristóbal-Hornillos, D.**[6], **Dupke, R.**[8], **Ederoclite, A.**[6], **Hernán-Caballero, A.**[6], **Hernández-Monteagudo, C.**[12] **López-Sanjuan, C.**[6], **Marín-Franch, A.**[6], **Mendes de Oliveira, C.**[13], **Moles, M.**[6], **Sodré Jr., L.**[13], **Taylor, K.**[14], **Varela, J.**[6], **Vázquez Ramió, H.**[6]

[1] Donostia International Physics Center (DIPC), Paseo Manuel de Lardizabal 4, 20018 Donostia-San Sebastian, Spain

[2] IKERBASQUE, Basque Foundation for Science, E-48013, Bilbao, Spain

[3] Observatório do Valongo, Ladeira Pedro Antonio, 43, Saude, Rio de Janeiro, 20080-090, BR

[4] Instituto de Astrofísica de Andalucía (IAA-CSIC), P.O. Box 3004, 18080 Granada, Spain

[5] INAF - Osservatorio di Astrofisica e Scienza dello Spazio di Bologna, via Gobetti 93/3, 40129 Bologna, Italy

[6] Centro de Estudios de Física del Cosmos de Aragón (CEFCA), Plaza San Juan 1, E–44001, Teruel, Spain

[7] Observatori Astronòmic de la Universitat de València, Ed. Instituts d'Investigació, Parc Científic. C/ Catedrático José Beltrán, n2, 46980 Paterna, Valencia, Spain

[8] Departament d'Astronomia i Astrofísica, Universitat de València, 46100 Burjassot, Spain

[9] Departamento de Física Matemática, Instituto de Física, Universidade de São Paulo, Rua do Matão, 1371, CEP 05508-090, São Paulo, Brazil

[10] Observatorio Nacional do Rio de Janeiro, Rua General José Cristino, 77, São Cristóvão, 20921-400, Rio de Janeiro, RJ, Brazil

[11] Instituto de Física, Universidade Federal da Bahia, 40210-340, Salvador, BA, Brazil

[12] Instituto de Astrofísica de Canarias (IAC), C. Vía Láctea, 38205 La Laguna, Santa Cruz de Tenerife, Spain

[13] Universidade de São Paulo, Instituto de Astronomia, Geofísica e Ciências Atmosféricas, Rua do Matão, 1226, 05508-090, São Paulo, SP, Brazil

[14] Instruments4, 4121 Pembury Place, La Canada Flintridge, CA 91011, U.S.A

Abstract

The Javalambre Physics of the Accelerating Universe Survey (J-PAS) has started observing wide areas of the northern sky with its unique set of 56 filters: 54 narrow band and 2 broader filters that cover the full optical range and effectively deliver a low-resolution spectrum for every object detected. Observations are carried out from the dedicated Javalambre Survey Telescope (JST/T250), based in the Observatorio Astrofísico de Javalambre (OAJ) and equipped with the wide field camera JPCam. The combination of the wide area coverage, the multi-band information and the high spatial resolution, make J-PAS an ideal survey not only for cosmological probes, but also for galaxy evolution studies. In this work we show the potential of J-PAS in the field of galaxy evolution by using "mini-JPAS", a small dataset of J-PAS-like data acquired during the testing phases of the JST/T250.

1   Introduction

Wide-area cosmological surveys deliver large datasets that allow studies across many fields in astronomy, on top of the analysis of the large-scale structure of the Universe. Combining the advantages that photometric and spectroscopic surveys provide, J-PAS is a unique large multi-band photometric survey designed to deliver low-resolution spectra for every object observed [3]. Being a photometric survey, J-PAS images all the sources in the target fields, where the only selection criteria is the limiting magnitude/depth of the detection band. Moreover, there are no biases resulting from the use of fixed apertures such as fibers or spectrographs. At the same time, its unique set of 56 filters involving narrow and intermediate bands covering the entire optical range effectively lead to a low-resolution spectroscopy (equivalent resolving power of $R \sim 60$ - See left panel of Fig. 1).

Here we show the potential of J-PAS in galaxy formation and evolution studies using the first data of the J-PAS collaboration, "mini-JPAS" [4]. In Section 2 we introduce the mini-JPAS dataset and in Section 3 we summarize all our results.

2   The miniJPAS dataset

The miniJPAS survey [4] is a precursor of the much larger J-PAS. It has been carried out with the temporary "Pathfinder" camera mounted on the JST/T250 telescope. The camera had a 9k × 9k CCD, a 0.3 square degree field of view, and a resolution of 0.23 arcseconds per pixel. miniJPAS includes observations of $\sim$1 deg^2 along the All-wavelength Extended Groth Strip International Survey (AEGIS) field [9] with the entire J-PAS filter system (54 narrow band + 2 intermediate band filters) plus 4 broad band filters (see right panel of Fig. 1). More than 64,000 sources are included in the miniJPAS catalog, with primary detection in the r-band, and forced photometry in all other bands (many more detections are available when extracting sources in the individual narrow-band images). miniJPAS is complete down
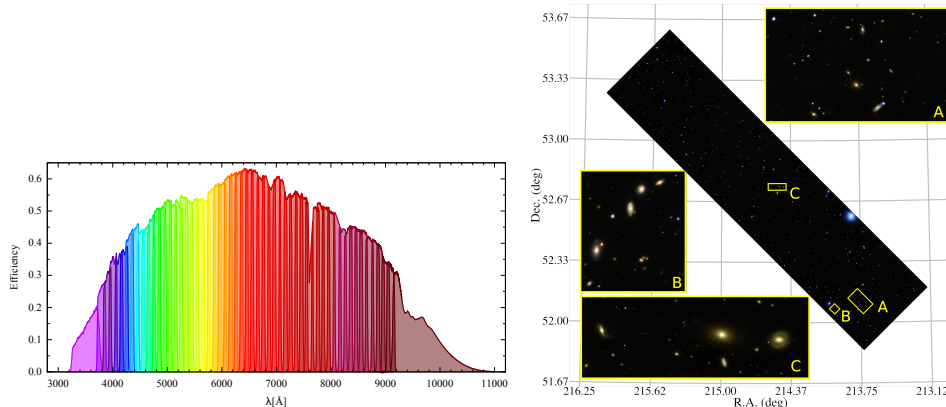
Figure 1: *Left panel*: J-PAS filter system. *Right panel*: coordinates and a g, r, i color image of miniJPAS, with thee zooms in selected regions. From [4].

to r = 23.6 AB for pointlike sources and r = 22.7 AB for extended sources [4]. The pseudo-spectra delivered are used not only to derive exquisite photometric redshifts [23], but also, among other things, to characterize the nature of the sources, derive their stellar population properties and detect emission lines, as discussed below.

3 Results

3.1 Global properties of galaxies

We conducted a preliminary study to test the potential of J-PAS-like data to constrain the stellar population properties of galaxies down to $z = 1$ and $r_{\mathrm{SDSS}} \leq 22.5$ AB (details in [21]). We put to test four SED-fitting codes especially developed for this aim by members of the J-PAS collaboration. We found that all the codes yield similar and compatible constraints on the age, metallicity, extinction, and stellar mass of miniJPAS galaxies. In fact, the precision of our results is comparable to the one obtained by spectroscopic surveys of similar signal-to-noise ratio. As expected, more massive miniJPAS galaxies are typically in the red-sequence and exhibit older and more metal-rich stellar populations than their counterparts in the blue-cloud (see Fig. 2). Finally, selecting galaxies at $0.05 < z < 0.15$, we performed a fossil-record approach of our SED-fitting results to demonstrate that we are able to track back the star formation rate density of galaxies up to $z \sim 3$ by solely using our data (see [21]).

Stellar mass and luminosity functions of galaxies are also key tools for setting constraints on cosmological models and the development of realistic mock catalogs, and hence, to discern among different scenarios of galaxy formation and evolution. Thanks to the stellar population properties constrained by our SED-fitting codes, we were able to explore the evolution of these functions up to $z \sim 0.7$ [18]. Our results revealed that the cosmic evolution of these functions in this redshift range mainly affects their massive/bright ends and the low-mass end of quiescent galaxies. In this regard, the global B-band luminosity density decreases by ~ 0.1 dex from $z = 0.7$ to 0.05, while the stellar mass density increases by 0.3 dex in the same
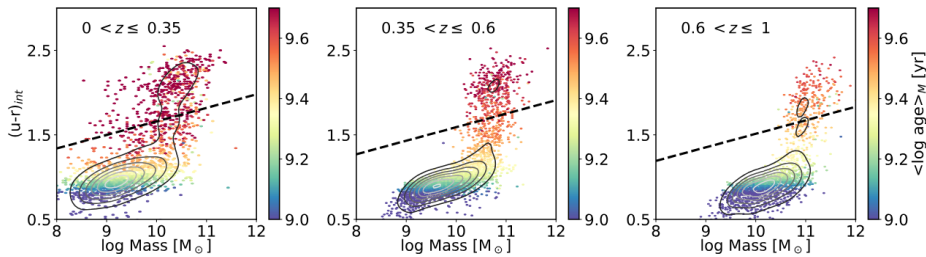
Figure 2: Stellar mass versus the rest-frame color corrected for extinction, $(u - r)_{int}$, diagram of miniJPAS galaxies at different redshifts. Dots are color-coded according to the mass-weighted ages obtained from the SED-fitting analysis. Figure from [21].
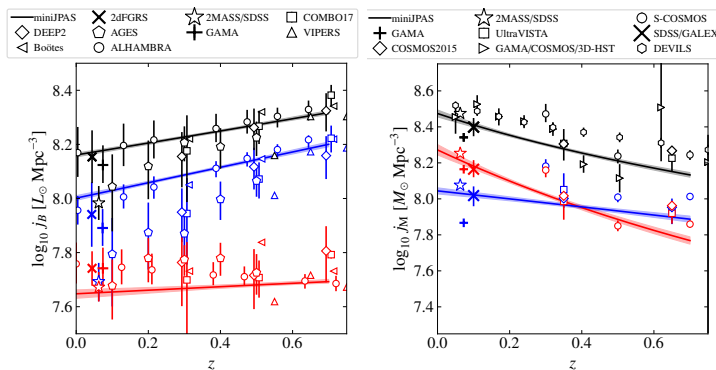

Figure 3: Evolution with redshift of the B-band luminosity and stellar mass densities of galaxies (*left and right panels*, respectively). The black, blue, and red solid lines illustrate the values for the full, star-forming, and quiescent samples of miniJPAS galaxies. Markers show values from previous works (see insets). Figure from [18].

redshift range (see left and right panels in Fig. 3, respectively). All this in good agreement with spectroscopic and deeper photometric surveys.

3.2 Nearby galaxies

The J-PAS filter system together with the high spatial resolution provided by the camera, also allows us to study the spatial variations of the properties of the stellar population of nearby galaxies, similarly to Integral Field Studies (IFS) but with the advantage of being able to reach larger galactocentric distances than traditional Integral Field Units (IFUs).

In [1], we studied the global properties of 32 X-ray selected Active Galactic Nuclei (AGN) host galaxies. The X-ray galaxies were selected using data from the Chandra X-ray Observatory [13, 14] and XMM-Newton [15], for which a full catalogue of X-ray AGN hosts in the miniJPAS field has been compiled by [29]. We obtained the stellar masses and SFR of the objects by fitting the SED of our samples using `CIGALE` [10, 11, 12]. Utilizing the IFU-like capabilities of miniJPAS, we explored the radial profiles of the SFR and sSFR of these AGN
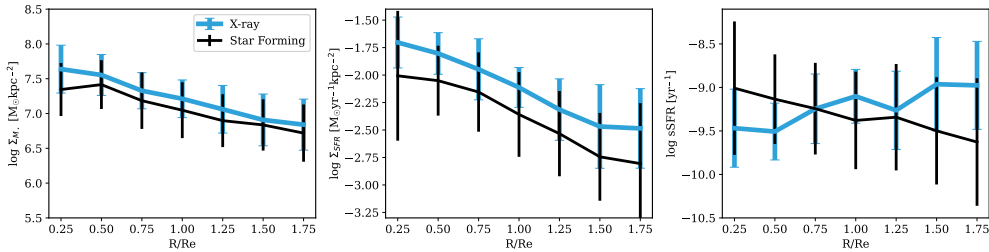
Figure 4: Radial profiles of the mass surface density ($\Sigma_{M_\star}$) (left), SFR surface density (Σ_{SFR}) (middle), and sSFR (right) for AGN and the mass-matched SF sample. Error bars represent the 3σ confidence intervals. Figure from [1].
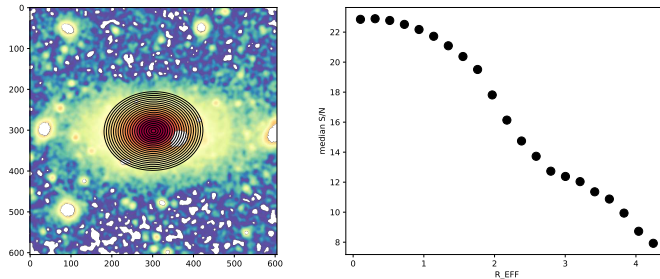

Figure 5: Example of results by Py2DJPAS. *Left panel*: an r_{SDSS} image, in log scale, after PSF homogenisation and masking. Black elliptical rings represent the segmentation used. *Right panel*: Median S/N in all the filters in each ring as a function of the distance to the galaxy centre.

and non-AGN host galaxies matched in stellar mass, by elliptically binning our samples using `piXedfit` [16, 17]. Our results, as shown in Fig. 4, indicate that X-ray AGN and SF galaxies show a different trend in their star forming radial profiles: the sSFR profiles of X-ray AGN tend to be increasing from the center to the outskirts of galaxies, and vice-versa in the case of SF galaxies. This leads us to a scenario where AGN do not significantly quench the host galaxies on a global scale, but only in the central regions, and enhance star formation in the outer regions.

In order to further exploit the IFU-like capability of J-PAS, we also have developed `Py2DJPAS`, a tool that automatizes the processes of analysis of the spatially resolved galaxies, including the download of the scientific images and tables, the masking and PSF homogenization of the images, the definition of the regions, and the calculation of their fluxes and magnitudes, using the calibration by [24, 25]. We have tested this code by retrieving the magnitudes provided in the catalogs, obtained with `SExtractor`, with a relative difference which is generally lower than a 10 % of the relative flux. This code has also allowed us to check that we are able to obtain J-PAS pseudo-spectrum with a high S/N, even at large distances from the galactic-centric distances (see Fig. 5). Additionally, we have used this code to study the role of the environment on the local properties of galaxies, finding no significant effect on our sample.
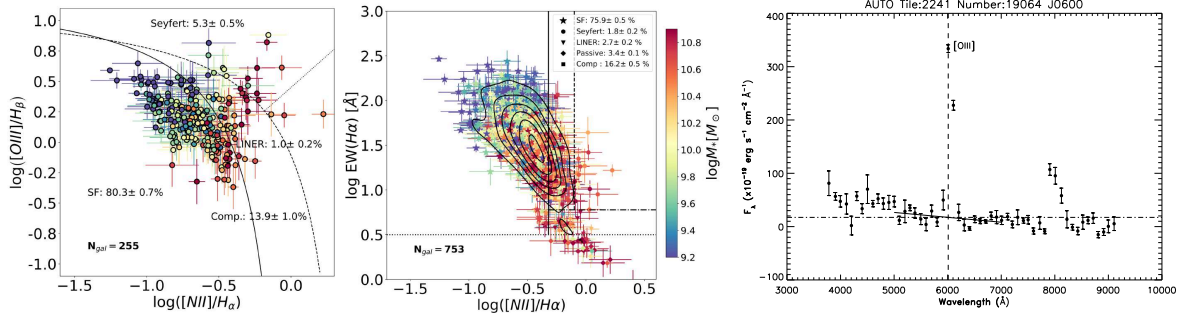
Figure 6: *Left*: BPT and *center*: WHAN diagrams for galaxies in miniJPAS ($0 < z < 0.35$) with error of 0.2 dex in the [O III]/Hβ and[N II]/Hα ratios. The color bar indicates the stellar mass of the galaxy. The solid (Ka03), dashed (Ke01), and dotted lines (S07) define the regions for the four main spectral classes. The relative percentage of each galaxy type in each subsample is indicated in the figure. In each panel, the number of galaxies is specified in the lower left corner. From [26]. *Right*: Photospectrum of one of the detected EELGs. The dashed vertical line indicates the central wavelength of the filter containing the [OIII] line. The dot dashed horizontal line shows the assumed underlying continuum at this wavelength.

3.3   Emission line galaxies and quasars

The photometric system of J-PAS enables also the detection of emission-line galaxies (ELGs) over a wide range of redshifts. Characterizing the ELG population across cosmic time and different environments is essential for understanding galaxy evolution, as star formation and AGN activity provide crucial insights into the fundamental processes governing galaxies. Therefore, predicting their emission lines is vital for inferring properties such as star formation rates, metallicities, and ionization conditions.

By means of artificial neural networks, we demonstrated in [27] that we can accurately predict the equivalent widths (EWs) of the main emission lines in the optical spectrum, such as Hβ, [O III], Hα, and [N II]. This is especially remarkable considering that [N II] and Hα are blended within the J-PAS photometric system. This technique has been applied to miniJPAS by [26]. In Fig. 6 (left), we present the predicted positions of galaxies in the BPT diagram for a subset of miniJPAS galaxies. The BPT diagram requires precise predictions of four emission lines, limiting our analysis to galaxies with high signal-to-noise ratios. However, we can utilize the WHAN diagram (center plot in Fig. 6) to determine the primary ionization mechanism for a larger sample of galaxies.

A search for extreme emission line galaxies (EELGs) was also conducted with the miniJ-PAS data in [28]. Defined as those galaxies that show equivalent widths $EW_0 \geq 300$Å in at least one of the emission lines [OII]$\lambda\lambda$3727,3729Å, [OIII]λ5007Å, and Hα, EELGs are dominated by strong bursts of young stars that ionize the gas surrounding them, and result in a spectrum featured by very intense emission lines on top of a faint continuum. These galaxies have been observed at different epochs of the Universe, although they are more frequent at high redshifts (e.g., [20]; [5]), and they could be responsible for a substantial fraction of the UV radiation required for the reionization of the Universe ([30]).

The miniJPAS instrumental setup is ideal to search for EELGs, since the strong emission lines of these galaxies are easily detected by comparing the flux detected with a given filter with those detected with the adjacent ones, and selecting those satisfying a contrast criterion that is equivalent to $EW_0 \geq 300$Å at a given emission line. This is illustrated in Fig. 6 (right), that shows the J-spectrum of one of the selected EELGs.

After discarding the QSOs, a total of 17 galaxies were classified as star-forming EELGs in the miniJPAS field; of these, 12 were detected in the [OIII] line, 2 in Hα, and 3 in both [OIII] and Hα. From a comparison with the [OIII] and Hα luminosity functions reported by [8], we estimate that we expect to detect galaxies below the characteristic L^* (i.e. low-luminosity galaxies) in the J-PAS survey at redshifts $z \leq 0.5$ in the [OIII] line, and $z \leq 0.25$ in the Hα line.

In a follow-up work, [6] performed a fit to the spectral energy distributions (SEDs) of the selected EELGs making use of a pipeline that combines photometric data from different archive facilities, spanning a wavelength range from the UV to the FIR. These SEDs are used as input for different evolutionary synthesis codes that provide as output basic properties of the EELGs as the total stellar mass or age. The obtained results are in good agreement with previous similar studies on samples of EELGs from SDSS, thus ensuring the reliability of this method, to be applied to the upcoming J-PAS data.
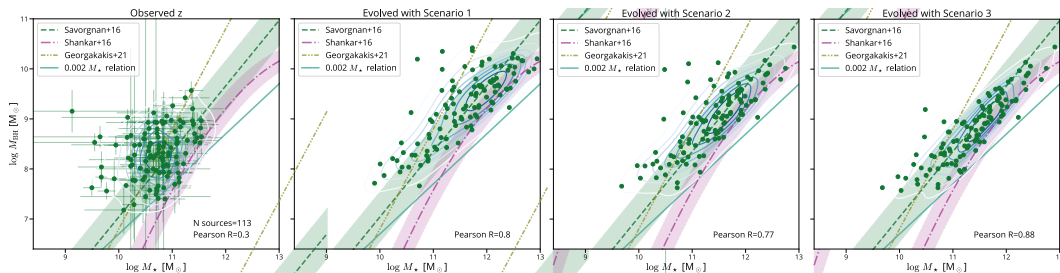

Figure 7: *First panel:* The observed M_{BH}–$M_\star$ relation for all the 113 sources in [29] at the observed redshift. Green solid dots are the value of masses for each source, with associated uncertainties, while contours are the distribution of these dots. In all panels, lines are different calibrations for the local M_{BH}–$M_\star$ relation, as labeled. The other three panels show the forward modeling of our sources to $z = 0$ using different methods. *Second panel:* the most basic model, with constant rates. *Third panel:* the model with a variable rate following the SFH. *Fourth panel:* the model with a variable rate following the SFH and the energy limit for the black hole accretion. We also show the number of sources and the Pearson correlation value in each bottom right corner. From [29].

With their strong and broad emission lines, quasars are also easily detected and characterized with the J-PAS filter system [2] and supermassive black hole (SMBH) masses can even be derived via the estimate of the emission line width [7].

In [29], we explore the coevolution of SMBHs with their host galaxies by studying a sample of X-ray-selected AGN out to z~2.5 within miniJPAS. Using SED fitting and single-epoch spectroscopy, we derived robust physical parameters for the host galaxies and the central SMBHs. The hardness ratio was used to estimate the X-ray obscuration. The SED fitting was done from photometric data from X-ray to infrared, using a large number of surveys on
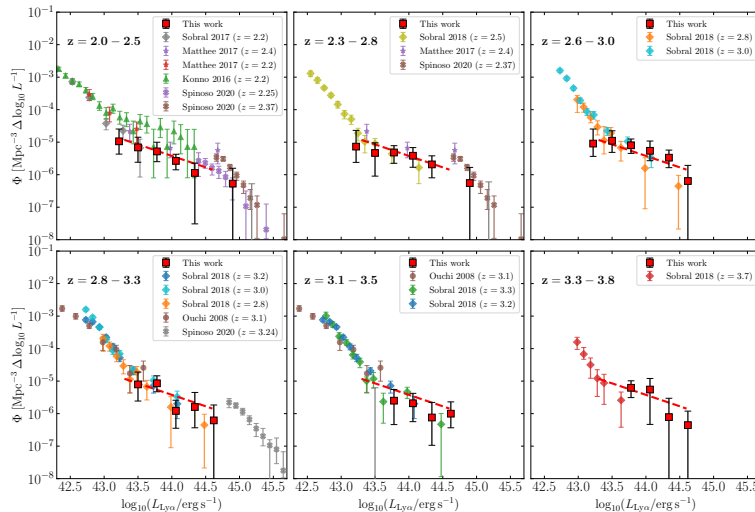
Figure 8: Lyman-α luminosity function of quasars in six bins of redshift, measured in 1.14 deg^2 of miniJPAS and J-NEP. Figure from [34].

top of the miniJPAS pseudo-spectra. The spectra fitting was done by carefully fitting the broad lines of each of these sources. We investigate three different evolutionary scenarios for the SMBH and host stellar masses by forward-modeling these sources until z=0 and compare them with the local scaling relation (see Fig. 7). From this analysis, we deduced that there is a shared connection between SFR and accretion, although this association is not present at all the moments in the entire cosmic evolutionary process. The best evolutionary scenario is when the SFR and accretion are coupled for the activity period but decouple completely when accretion expels so much energy that it can tear apart the galaxy.

In [34] we developed a method to detect Lyman-α emitters (LAEs) using the J-PAS filter system to estimate the Lyα luminosity function (LF) within $2.05 < z < 3.75$. To refine this method, we constructed a mock catalog comprising quasars ($0 < z < 4.2$), star-forming LAEs ($z > 2$), and low-z galaxies. The mocks were utilized to build two-dimensional maps of purity and number count corrections, improving the accuracy of the Lyα LF estimate. We identified 67 LAE candidates within $2.05 < z < 3.75$, achieving $>75\%$ completeness and $>60\%$ purity at $L_{\text{Ly}\alpha} \gtrsim 10^{43.75}$ erg s^{-1}, with purity reaching $\sim 100\%$ at $L_{\text{Ly}\alpha} \gtrsim 10^{44}$ erg s^{-1} and $z \gtrsim 3$. The resulting Lyα LF shows consistency with previous studies. With forthcoming J-PAS data covering a few hundred square degrees, this method will allow us to resolve the Lyα LF in redshift bins of $\Delta z = 0.12$ across $L_{\text{Ly}\alpha} = 10^{43.5-45}$ erg s^{-1} for $z = 2$–6.

While searching extended Lyα nebulosities around high redshift quasars (z>2) using miniJPAS observations, we discovered two QSOs: SDSS J141935.58+525710.7 at z=3.218 (hereafter QSO1) and SDSS J141813.40+525240.4 at z=3.287 (hereafter QSO2) exhibiting double-cored Lyα emission (See Figure 9) in at least one of the NB filters that contain Lyα (J0510/J0520 for QSO1 and J0520/J0530 for QSO2) [32]. The separations between the two Lyα cores are 11.07 ± 2.26 kpc and 9.73 ± 1.55 kpc with Lyα line luminosities of $\sim 3.35 \times 10^{44}$ erg s^{-1} and $\sim 6.99 \times 10^{44}$ erg s^{-1} for QSO1 and QSO2, respectively. It is extremely
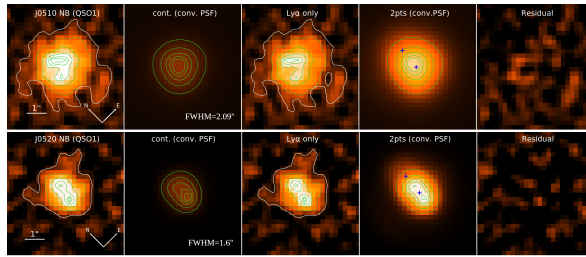
Figure 9: QSO1 images in two Lyα NB J-PAS filters. From left to right: (1) NB miniJPAS; (2) PSF-convolved continuum; (3) Lyα continuum-subtracted; (4) two-point PSFs convolved with Lyα flux; (5) residual image after two-point PSF subtraction from Lyα image. Blue crosses mark PSF centers from GALFIT, white contours (1,3) show 2σ isophote above background STD, while green contours represent 30%, 60%, 80%, 90%, and 95% of peak values. FWHM size of PSFs is noted in (2). From [32].

rare to find such bright, double-cored Lyα nebulae in relatively shallow narrow-band images, especially given the lack of evidence that these are binary quasars (only one continuum component is seen). Analysis of J-PAS filter images covering HeII, CIV, CIII] emission lines, the UV line ratios (CIV/Lyα and HeII/Lyα) and QSO spectral properties suggests that a combination of resonant scattering and galactic outflows play a major role in powering the double-cored Lyα emission.

3.4 Galaxies and their environment

The combination of the J-PAS filter system, that allows for the retrieval of the stellar population of properties of galaxies [21], and the large FoV, that allows for unbiased galaxy clusters and groups detection (see [19, 31]) make J-PAS an excellent survey to also study the role of environment on galaxy evolution. In fact, the works by [22, 33] have proven these capabilities by using the cluster and groups catalogs by [31] and de SED-fitting code `BaySeAGal` (de Amorim et al., in prep.; see al so [21]).

The role of group environment on quenching the star formation was studied by [22]. In this work, we first divided miniJPAS galaxies into those in groups and those in the field, using the probabilistic association, P_{assoc} provided in the catalogs by [31] for 80 galaxy groups at $z \leq 0.8$. Using the results from the SED-fitting, particularly the $(u - r)_{int}$ color, the stellar mass $M_\star$, and the specific star formation rate (sSFR), we also classified galaxies into red/blue galaxies and quiescent/star-forming/transition galaxies. Our results shows a clear dependency of the aforementioned galaxy populations with the stellar mass and the environment (see Fig. 10). In particular, the fraction red galaxies increases with $M_\star$ and is larger for groups (28 % on average) than in the field (5 % on average). However, the shift in the distribution of the properties is mostly due to the different fraction of red and blue galaxies in groups and in the field. We found a strong dependence of the quenched fraction excess in groups with mass, but the dependence of the abundance excess of transition galaxies in groups with the mass is more modest. Our results also show that the time that galaxies in groups spend in the transition phase is lower than 1.5 Gyr, which implies that galaxies are
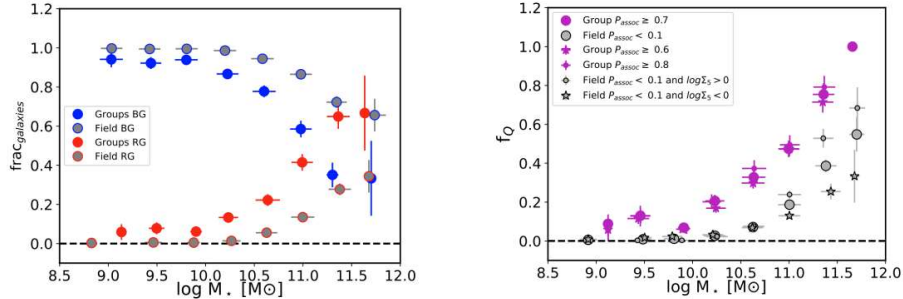
Figure 10: Fraction of red, blue and quenched galaxies as a function of the galaxy's stellar mass and environment. *Left panel*: fraction of blue and red galaxies (red and blue markers, respectively). Color points for the field, gray point for groups. *Right panel*: fraction of quenched galaxies. Magenta/gray markers represent galaxies in groups/in the field. Figure from [22]

quenched very quickly in groups, but we find that the cluster environment is noticeably more efficient at quenching galaxies than groups. Lastly the galaxy quenching rate evolves modestly with redshift. The general picture drawn by our results is compatible with an scenario were low-mass star forming galaxies in clusters are quenched at $z \sim$ 1-4, in agreement with the references found in [22].

Similarly, the work carried out by [33] focuses in studying the galaxy populations in the most massive cluster in miniJPAS: mJPC2470-1771. This cluster is at $z = 0.29$, with coordinates $(\alpha, \delta) = (213°.6254, +51°.9379)$. Its R_{200} is 1304 kpc and its $M_{200} = 3.3 \times 10^{14}$ $M_{\odot}$. Using the catalogs by [31], we select a total of 96 galaxies in the cluster. Using the stellar population properties and star formation histories obtained using `BaySeAGal`, as well as the estimation of the equivalent widths of the Hα, Hβ, [NII], and [OIII] emission lines, obtained with the ANN from [27], we were able to classify galaxies into red and blue galaxies, select those galaxies with emission lines (49 galaxies in total), and classify this subsample into star-forming galaxies (65.3 %), AGN hosts (24 %), and galaxies with a composite behavior (10.7 %). This classification, combined with the miniJPAS FoV, allowed us not only to study the galaxy populations and the stellar population properties of the galaxies in the cluster, but also their spatial and radial distribution (see Fig. 11). Our results show that the fraction of red galaxies in the cluster (0.52) is almost the double than the fraction of red galaxies in the whole miniJPAS catalog. This fraction, as well as the fraction of AGN hosts, increases towards the central regions of the cluster, at the same time that the fraction of blue and star forming galaxies decreases. Similarly, the median sSFR of the cluster decreases towards the central regions of the cluster. However, we find that properties of red galaxies are very similar at all cluster-centric distances, while blue galaxies become, redder, more massive and older, with lower sSFR, towards central regions. Regarding the star formation history, our results imply that all galaxies were formed at a similar epoch, but red galaxies had shorter and faster star formation episodes. The general picture drawn by our results is compatible with a
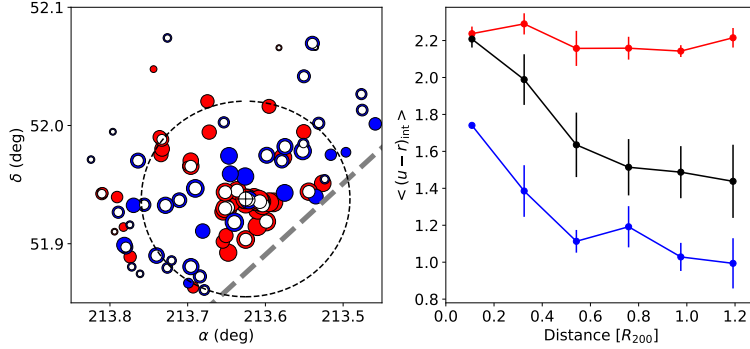
Figure 11: Distribution of the galaxy populations in the cluster mJPC2470-1771. *Left panel*: Spatial distribution of red, blue, and emission line galaxies (red, blue, and white points, respectively). Black dashed circle represents R_{200}. Grey dashed line represents the limit of the footprint. *Right panel*: radial profile of the median $(u-r)_{int}$ color for red, blue and all galaxies (red, blue, and black profiles, respectively). Figure from [33].

pre-processing scenario, where galaxies were quenched prior or during the cluster accretion.

Acknowledgments

References

[1] Acharya, N., Bonoli, S., Salvato M., Cortesi A., González Delgado, R. M. et al. 2024, A&A, 687, A285

[2] Abramo, L. R., Strauss, M. A., Lima, M., et al. 2012, , 423, 3251. doi:10.1111/j.1365-2966.2012.21115.x

[3] Benitez, N., Dupke, R., Moles, M., et al. 2014, arXiv:1403.5237. doi:10.48550/arXiv.1403.5237

[4] Bonoli, S., Marín-Franch, A., Varela, J., Vázquez Ramió, H., et al. 2021, A&A, 653, A31

[5] Boyett, K. N. K., Stark, D. P., Bunker, A. J., et al. 2022, MNRAS, 513, 4451

[6] Breda, I., Amarantidis, S., Vilchez, J. M., et al. 2024, MNRAS, 528, 3340

[7] Chaves-Montero, J., Bonoli, S., Trakhtenbrot, B., et al. 2022, , 660, A95. doi:10.1051/0004-6361/202142567

[8] Comparat, J., Zhu, G., Gonzalez-Perez, V., et al. 2016, MNRAS, 461, 1076

[9] Davis, M., Guhathakurta, P., Jonidaris, N.P, et al. 2007, ApJL, 660, L1

[10] Boquien, M., Burgarella, D., Roehlly, Y., et al. 2019, A&A, 622, A103

[11] Yang, G., Boquien, M., Buat, V., et al. 2020, MNRAS, 491, 740–759

[12] Yang, G., Boquien, M., Brandt, W.N., et al. 2022, MNRAS, 590, 1250–1273

[13] Laird, E. S., Nandra, K., Georgakakis, A., et al. 2009, ApJSS, 180, 102

[14] Nandra, K., Laird, E. S., Aird, J. A., et al. 2015, ApJSS, 220, 10

[15] Liu, T., Merloni, A., Simm, T., et al. 2020, TAPJSS, 250, 32

[16] Abdurro'uf & Akiyama, M. 2017, MNRAS, 469, 2806

[17] Abdurro'uf, Lin, Y.-T., Wu, P.-F., & Akiyama, M. 2021, ApJSS, 254, 15

[18] Díaz-García, L.A., González Delgado, R.M., García-Benito, R., et al. 2024, A&A, 688, A113

[19] Doubrawa, L., Cypriano, E. S., Finoguenov, A., et al. 2023, MNRAS, 526, 4285

[20] Endsley, R., Stark, D. P., Chevallard, J., et al. 2021, MNRAS, 500, 5229

[21] González Delgado, R. M., Díaz-García, L. A., de Amorim, A., et al. 2021, A&A, 649, A79

[22] González Delgado, R. M., Rodríguez-Martín, J. E., Díaz-García, L. A., et al. 2022, A&A, 666, A84

[23] Hernán-Caballero, A. and Varela, J. and López-Sanjuan, C. and Muniesa, D. and Civera, T. et al. 2023, A&A, 654, A101

[24] López-Sanjuan, C., Varela, J., Cristóbal-Hornillos, D., et al. 2019, A&A, 631, A119

[25] Vázquez Ramió, H., Xiao, K., et al. 2024, A&A, 683, A29

[26] G. Martínez-Solaeche, R. M. González Delgado, R. García-Benito et al. 2022, A&A, 661, A99

[27] G. Martínez-Solaeche, R. M. González Delgado, R. García-Benito et al. 2021, A&A, 647, A158

[28] Iglesias-Páramo, J., Arroyo, A., Kehrig, C., et al. 2022, A&A, 665, A95

[29] López, I.E., Brusa, M., et al. 2023, A&A 672, A137

[30] Matthee, J., Naidu, R. P., Pezzulli, G., et al. 2022, MNRAS, 512, 5960

[31] Maturi, M., Finoguenov, A., Lopes, P. A. A., et al. 2023, A&A, 678, A145

[32] Rahna, P. T., Zheng, Z. -Y., Chies-Santos, A. L. et al. 2022, A&A,668, A148

[33] Rodríguez-Martín, J. E., González Delgado, R. M., Martínez-Solaeche, G., et al. 2022, A&A, 666, A160

[34] Torralba-Torregrosa, A., Gurung-López, S., Arnalte-Mur, P., et al. 2023, A&A, 680, A14